1521-0103/364/1/131–144$25.00
THE JOURNAL OF PHARMACOLOGY AND EXPERIMENTAL THERAPEUTICS

https://doi.org/10.1124/jpet.117.243162
J Pharmacol Exp Ther 364:131–144, January 2018

K_V7 Channel Pharmacological Activation by the Novel Activator ML213: Role for Heteromeric $K_V7.4/K_V7.5$ Channels in Guinea Pig Detrusor Smooth Muscle Function[S]

Aaron Provence, Damiano Angoli, and Georgi V. Petkov

Department of Drug Discovery and Biomedical Sciences, South Carolina College of Pharmacy, University of South Carolina, Columbia, South Carolina (A.P., D.A., G.V.P.); and Department of Pharmaceutical Sciences, College of Pharmacy, University of Tennessee Health Science Center, Memphis, Tennessee (G.V.P.)

Received June 2, 2017; accepted October 20, 2017

ABSTRACT

Voltage-gated K_V7 channels ($K_V7.1$ to $K_V7.5$) are important regulators of the cell membrane potential in detrusor smooth muscle (DSM) of the urinary bladder. This study sought to further the current knowledge of K_V7 channel function at the molecular, cellular, and tissue levels in combination with pharmacological tools. We used isometric DSM tension recordings, ratiometric fluorescence Ca^{2+} imaging, amphotericin-B perforated patch-clamp electrophysiology, and in situ proximity ligation assay (PLA) in combination with the novel compound *N*-(2,4,6-trimethylphenyl)-bicyclo[2.2.1]heptane-2-carboxamide (ML213), an activator of $K_V7.2$, $K_V7.4$, and $K_V7.5$ channels, to examine their physiologic roles in guinea pig DSM function. ML213 caused a concentration-dependent (0.1–30 μM) inhibition of spontaneous phasic contractions in DSM isolated strips; effects blocked by the K_V7 channel inhibitor XE991 (10 μM). ML213 (0.1–30 μM) also reduced pharmacologically induced and nerve-evoked contractions in DSM strips. Consistently, ML213 (10 μM) decreased global intracellular Ca^{2+} concentrations in Fura-2–loaded DSM isolated strips. Perforated patch-clamp electrophysiology revealed that ML213 (10 μM) caused an increase in the amplitude of whole-cell K_V7 currents. Further, in current-clamp mode of the perforated patch clamp, ML213 hyperpolarized DSM cell membrane potential in a manner reversible by washout or XE991 (10 μM), consistent with ML213 activation of K_V7 channel currents. Preapplication of XE991 (10 μM) not only depolarized the DSM cells, but also blocked ML213-induced hyperpolarization, confirming ML213 selectivity for K_V7 channel subtypes. In situ PLA revealed colocalization and expression of heteromeric $K_V7.4/K_V7.5$ channels in DSM isolated cells. These combined results suggest that ML213-sensitive $K_V7.4$- and $K_V7.5$-containing channels are essential regulators of DSM excitability and contractility.

Introduction

Voltage-gated K_V7 channels ($K_V7.1$ to $K_V7.5$), encoded by *KCNQ* genes (*KCNQ1* to *KCNQ5*), are critically involved in establishing and maintaining the cell membrane potential of many excitable cells and tissue types (Jepps et al., 2009; Ng et al., 2011; Brueggemann et al., 2012a, 2014b; Evseev et al., 2013; Mani et al., 2013; Stott et al., 2014). In addition, emerging new evidence points to potential physiologic roles for the K_V7 channels in detrusor smooth muscle (DSM), the main muscular component of the urinary bladder (Streng et al., 2004; Rode et al., 2010; Afeli et al., 2013; Anderson et al., 2013; Svalø et al., 2013, 2015; Stott et al., 2014; Provence et al., 2015; Mani et al., 2016).

Recent studies from our laboratory and others show that K_V7 channels serve key functional roles in regulating DSM function in rats (Rode et al., 2010; Svalø et al., 2013), guinea pigs (Afeli et al., 2013; Anderson et al., 2013; Provence et al., 2015), pigs (Svalø et al., 2013), and humans (Svalø et al., 2015; Bientinesi et al., 2017). K_V7 channel activation leads to hyperpolarization of the membrane potential, thereby decreasing Ca^{2+} influx through L-type voltage-gated Ca^{2+} channels, which precludes Ca^{2+}-dependent activation of myosin light chain kinase necessary for the initiation of DSM contractility (Petkov, 2011; Stott et al., 2014). K_V7 channels were initially termed "M channels" as pioneering studies in frog sympathetic neurons demonstrated the suppression of K_V7 channel currents in response to $G_{q/11}$-coupled muscarinic acetylcholine receptor (mAChR) activation (Brown et al., 1980). However, whether mAChRs are involved in the regulation of K_V7 channel activity in DSM is not known.

K_V7 channel pore-forming α-subunits ($K_V7.1$ to $K_V7.5$) have been shown to form both homomeric and heteromeric channel conformations in experimental cell lines and native biologic

This study was supported by a grant from the National Institutes of Health R01 DK106964 to Georgi V. Petkov. Aaron Provence was supported by an NIH pre-doctoral fellowship F31 DK104528 under Dr. Petkov's mentorship.
https://doi.org/10.1124/jpet.117.243162.
[S] This article has supplemental material available at jpet.aspetjournals.org.

ABBREVIATIONS: BK, large-conductance voltage-activated and Ca^{2+}-activated K^+ channel; CCh, carbachol; DSM, detrusor smooth muscle; EFS, electrical field stimulation; ICA-069673, *N*-(2-chloro-5-pyrimidinyl)-3,4-difluorobenzamide; IP_3R, inositol triphosphate receptor; K_V, voltage-gated K^+ channel; mAChR, muscarinic acetylcholine receptor; ML213, N-(2,4,6-Trimethylphenyl)-bicyclo[2.2.1]heptane-2-carboxamide; PLA, proximity ligation assay; TTX, tetrodotoxin; XE991, 10,10-*bis*(4-pyridinylmethyl)-9(10H)-anthracenone dihydrochloride.

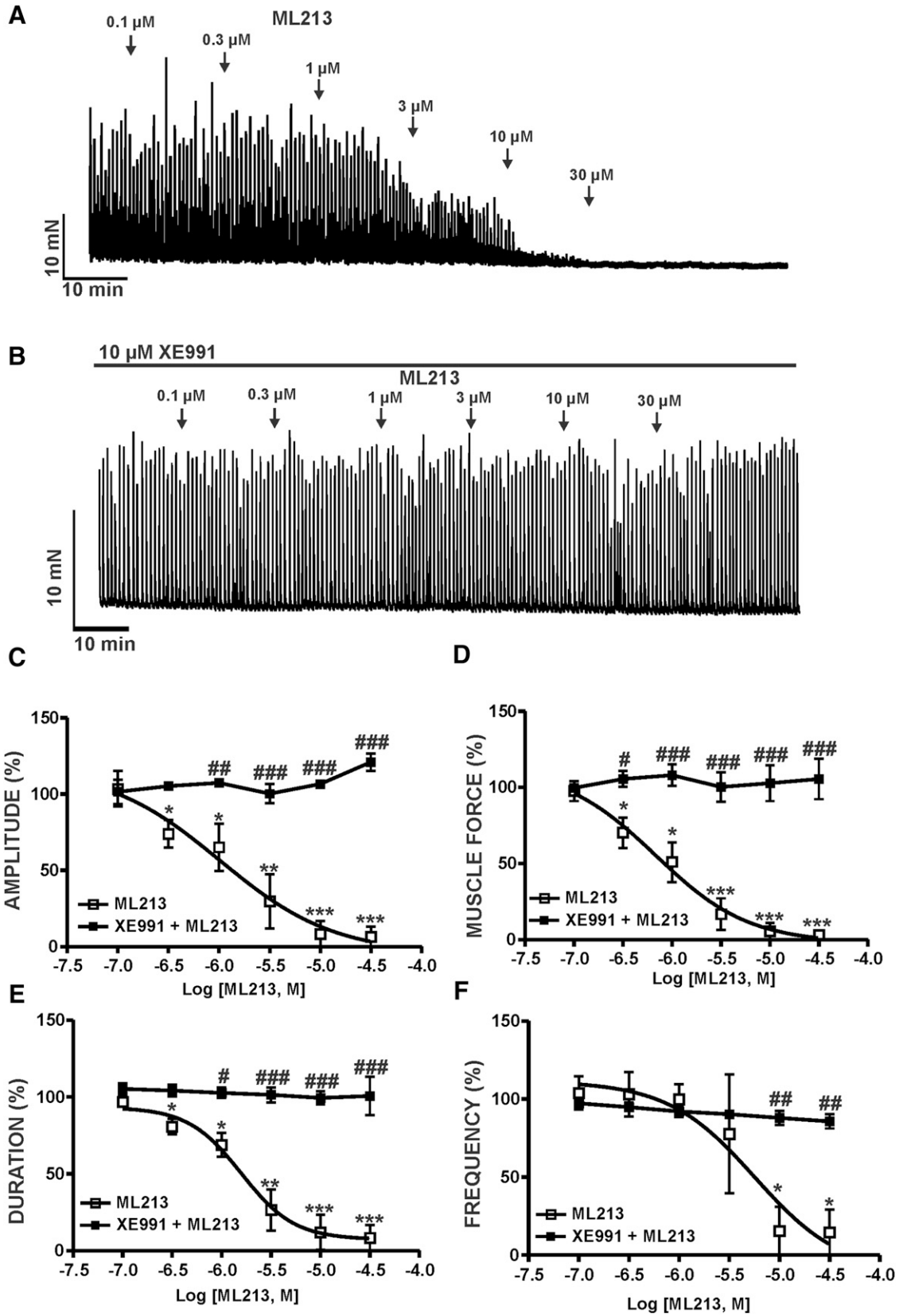

Fig. 1. K_V7 channel pharmacological activation with ML213 leads to an inhibition of spontaneous phasic contractions in DSM isolated strips. (A) A representative isometric DSM tension recording demonstrating that ML213 (0.1–30 μM) inhibited spontaneous phasic contractions in a DSM isolated strip. (B) A representative isometric DSM tension recording illustrating the K_V7 channel inhibitor XE991 (10 μM) abolished the inhibitory effects of ML213 (0.1–30 μM) on DSM spontaneous phasic contractions. Cumulative concentration-response curves for ML213 on DSM phasic contraction: amplitude (C), muscle force (D), duration (E), and frequency (F) in the absence and presence of the K_V7 channel inhibitor XE991 at 10 (micro)M ($n = 6, N = 6$; $^*P < 0.05$; $^{**}P < 0.01$; $^{***}P < 0.001$). $\#P < 0.05$; $\#\#P < 0.01$; $\#\#\#P < 0.001$ indicate statistical significance in the effects of ML213 on spontaneous phasic contractions in the absence (control) versus the presence of XE991 ($n = 6, N = 6$; two-way ANOVA followed by Bonferroni post-test). See Table 1 for potency and maximum efficacy values and Supplemental Fig. 1 for the illustration of concentration responses, data for which are shown as the mean ± S.D.

TABLE 1

IC_{50} and maximal efficacy values for the effects of ML213 on spontaneous phasic, KCl-induced (20 mM), CCh-induced (0.1 or 1 μM), and EFS-induced (10 or 20 Hz) phasic contractions in guinea pig DSM isolated strips

IC_{50} values are presented as the mean (95% confidence interval). Maximal efficacy is presented as the mean ± S.E.M. and is normalized to the control on a scale from 100% to 0% (full relaxation); n/a=not applicable (negligible effect on parameter).

Condition	Amplitude	Muscle Force	Duration	Frequency	*n/N*
Spontaneous phasic contractions	1.1 (0.5–2.4) μM; 95.6% ± 4.4%	0.7 (0.2–2.8) μM; 96.8% ± 3.2%	1.6 (0.8–2.9) μM; 91.6% ± 8.41%	3.9 (0.8–20.3) μM; 85.4% ± 14.6%	6/6
KCl (20 mM)-induced contractions	2.7 (1.4–5.1) μM; 99.2% ± 0.8%	2.5 (1.2–5.3) μM; 99.1% ± 0.9%	3.9 (1.9–8.2) μM; 90.3% ± 9.7%	n/a; 87.6% ± 8.2%	7/7
CCh (0.1 μM)-induced contractions	3.5 (1.9–6.4) μM; 100% inhibition	2.1 (1.1–3.9) μM; 100% inhibition	3.0 (1.8–5.3) μM; 99.7% ± 0.29%	n/a; 100% inhibition	6/6
CCh (1 μM)-induced contractions	6.2 (1.2–30.7) μM; 84% ± 9.1%	4.4 (0.8–22.3) (micro)M; 92.1% ± 4.2%	11.3 (2.1–61.2) (micro)M; 68% ± 9.5%	n/a; 47.1% ± 15.4%	6/6
10-Hz EFS-induced contractions	2.2 (1.3–3.7) μM; 83.6% ± 7.6%	2.3 (1.3–4.1) μM; 83.9% ± 8.2%	n/a; 32.78% ± 13.5%	n/a	7/6
20-Hz EFS-induced contractions	5.1 (3.1–8.2) μM; 86.9% ± 6.4%	4.7 (2.7–8.1) μM; 89.1% ± 6.0%	n/a; 37.46% ± 9.3%	n/a	6/6

systems, which significantly expands the molecular and functional diversity of the K_V7 channel family (Abbott and Goldstein, 2001; Wrobel et al., 2012). Further, K_V7 channel expression and function have also been shown to follow a certain level of subtype and tissue specificity. For example, $K_V7.1$ channels have established roles in the repolarization of the cardiac action potential (Barhanin et al., 1996), heteromeric $K_V7.2/K_V7.3$ channels underlie the neuronal "M current" (Brown and Passmore, 2009), and homomeric or heteromeric combinations of $K_V7.4$ and $K_V7.5$ channel subtypes appear to be most critical in smooth muscle function (Haick and Byron, 2016). Understandably, the development of

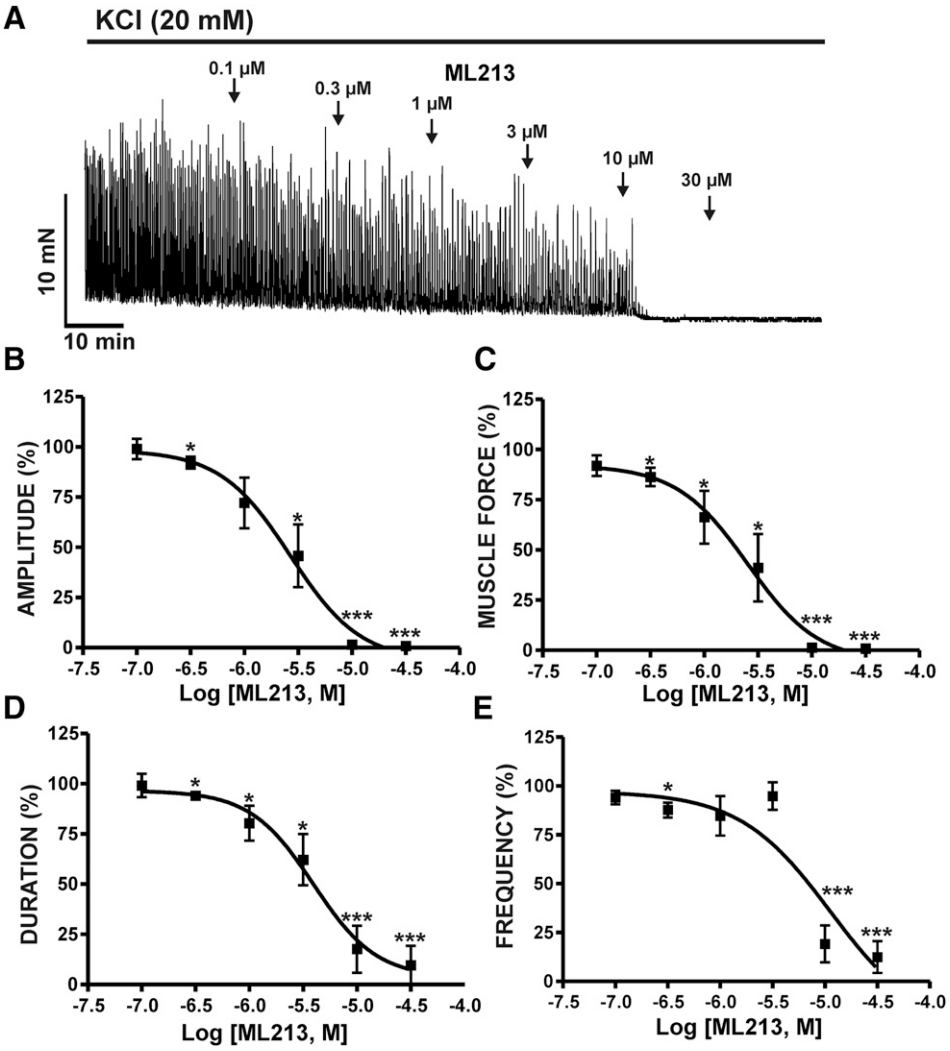

Fig. 2. K_V7 channel pharmacological activation with ML213 leads to an inhibition of 20 mM KCl-induced phasic contractions in DSM isolated strips. (A) A representative isometric DSM tension recording demonstrating the concentration-dependent inhibition of 20 mM KCl-induced DSM phasic contractions by ML213 (0.1–30 μM). Cumulative concentration-response curves for the inhibitory effects of ML213 on DSM phasic contraction: amplitude (B), muscle force (C), duration (D), and frequency (E) ($n = 7, N = 7$; $^*P < 0.05$; $^{***}P < 0.001$; two-tailed paired Student's *t*-test). See Table 1 for potency and maximum efficacy values and Supplemental Fig. 2 for illustration of summary concentration-responses, data for which are shown as the mean ± S.D.

novel K_V7 channel pharmacological modulators, with improved selectivity to distinguish among individual K_V7 channel subtypes, is a highly sought endeavor. Indeed, several K_V7 channel pharmacological modulators have emerged in recent years displaying improved selectivity for individual K_V7 channel subtypes, including the $K_V7.2/K_V7.3$ channel activator ICA-069673 [*N*-(2-chloro-5-pyrimidinyl)-3,4-difluorobenzamide], a potent inhibitor of DSM excitability and contractility (Provence et al., 2015).

The compound *N*-(2,4,6-trimethylphenyl)-bicyclo[2.2.1]-heptane-2-carboxamide (ML213) is a novel K_V7 channel activator initially characterized as being selective for $K_V7.2$ and $K_V7.4$ channel subtypes displaying ~80-fold selectivity over other K_V7 channels (Yu et al., 2010, 2011), as well as greater potency than other Kv7 activators such as retigabine and BMS 204352 [(3S)-(+)-(5-chloro-2-methoxyphenyl)-1,3-dihydro-3-fluoro-6-(trifluoromethyl)-2H-indole-2-one] (Jepps et al., 2014). Subsequent in vitro pharmacological and electrophysiological studies in A7r5 vascular smooth muscle cells have reported ML213 as a potent activator of homomeric $K_V7.4$ and $K_V7.5$ channels and heteromeric $K_V7.4/K_V7.5$ channels (Brueggemann et al., 2014a). ML213 is currently the only known K_V7 channel activator with this unique pharmacological selectivity profile. Nonetheless, studies seeking to identify whether heteromeric K_V7 channels, specifically heteromeric $K_V7.4/K_V7.5$ channels, are expressed in DSM are currently absent. To identify the potential ML213-sensitive K_V7 channel conformations expressed at the cellular level in DSM would greatly enhance our understanding of ML213 pharmacological effects on DSM function, while expanding our knowledge of the physiologic roles of K_V7 channel subtypes in the urinary bladder.

Here, we used the novel K_V7 channel activator ML213 to reveal insights into the subtype-specific K_V7 channel functional roles in DSM excitability and contractility. This was achieved by a multidisciplinary experimental approach using isometric DSM tension recordings, ratiometric fluorescence Ca^{2+} imaging, and amphotericin-B perforated patch-clamp electrophysiology. Further, in situ proximity ligation assay (PLA) was conducted to elucidate whether $K_V7.4$ and $K_V7.5$ channels, key pharmacological targets of ML213, colocalize to form heteromeric channel complexes in DSM cells.

Materials and Methods

Ethical Approval for Animal Use. Protocols for the use of experimental animals in the current study are consistent with the National Institutes of Health Guidelines for the Care and Use of Experimental Animals and were reviewed and approved by the Institutional Animal Care and Use Committee (IACUC) of the University of South Carolina, Columbia, SC (protocols #2186-100859-072114 and #2321-101157-092116).

Animal Housing, Euthanization, and DSM Tissue Acquisition. Forty-one adult male Hartley-Albino guinea pigs (Charles River Laboratories, Raleigh, NC), 3–12 months of age and weighing 341–1191 g (average weight, 902 ± 10 g), were used for this study. Animals were housed in the Animal Resource Facilities at the University of South Carolina where they had free access to food and water and were exposed to 12-hour light/dark cycles at room temperature (22–23°C). Animals were euthanized via CO_2 inhalation using a SMARTBOX Automated CO_2 Delivery System (Euthanex Corp., Palmer, PA), followed by thoracotomy. The urinary bladder was then removed by an incision superior to the bladder neck. After dissection, the urinary bladder was cut open via a longitudinal incision originating from the urethral orifice. This allowed the bladder to be opened and pinned down flat to the base of a Sylgard-coated (Dow Corning, Corning, NY) Petri dish. Under a dissection microscope, microscissors and forceps were used to remove the entire mucosal layer and lamina propria, including the urothelium.

DSM Cell Isolation and Collection. DSM single cells were freshly isolated using a combination of papain and collagenase, as previously described (Hristov et al., 2012b). DSM cells were used for electrophysiological experiments or in situ PLA within 12 hours after isolation. Intact DSM strips with urothelium removed were used for single-cell isolation, isometric DSM tension recordings, and ratiometric fluorescence Ca^{2+} imaging.

Isometric DSM Tension Recordings. Isometric DSM tension recordings were conducted as previously described on isolated DSM strips void of urothelium (Hristov et al., 2012b). For experiments on spontaneous phasic, carbachol (CCh)-induced, and KCl-induced contractions, the DSM isolated strips were pretreated with the neuronal voltage-gated Na^+ channel blocker tetrodotoxin (TTX; 1 μM) before the concentration-response effects of ML213 (0.1–30 μM) were assessed. Electrical field stimulation (EFS)–induced DSM contractions were stimulated with a PHM-152I programmable stimulator (Med Associates, Inc., Geogia, VT) in the absence of TTX. A 10- or 20-Hz EFS frequency, respectively, was delivered at 1-minute intervals, and ML213 (0.1–30 μM) was administered once a stable baseline and a contraction amplitude were achieved. In a separate protocol, EFS-induced DSM contractions were stimulated at 3-minute intervals over a wide range of frequencies (0.5, 2.0, 3.5, 5, 7.5, 10, 12.5, 15, 20, 30, 40, and 50 Hz) in the absence (control) and then in the presence of ML213 (1 or 3 μM). The inhibitory effects of ML213 were normalized to

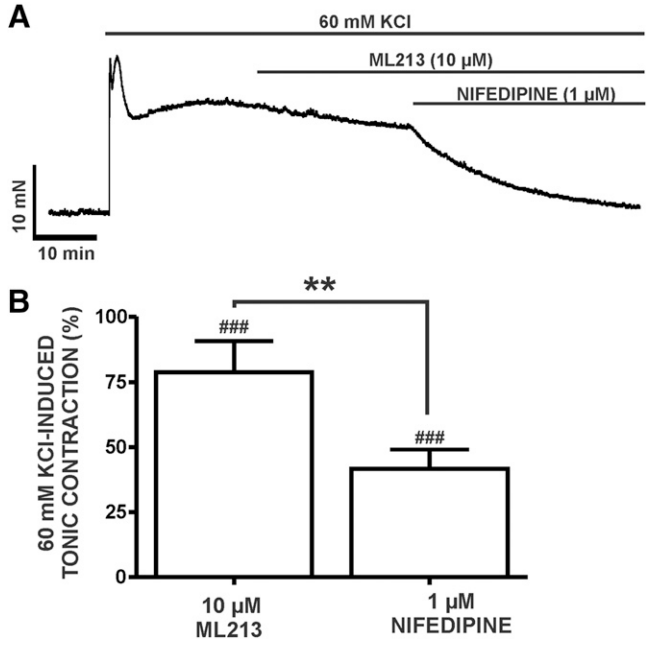

Fig. 3. Differential inhibitory effects of ML213 and nifedipine on 60 mM KCl-induced tonic contractions in DSM isolated strips. (A) A representative isometric DSM tension recording demonstrating the differential effects of 10 μM ML213 and 1 μM nifedipine upon a depolarization-induced DSM tonic contraction caused by 60 mM KCl in a DSM isolated strips. (B) Summarized data demonstrating the differential inhibitory effects of ML213 (10 μM) and nifedipine (1 μM) + ML213 on DSM 60 mM KCl-induced tonic contraction (n = 8, N = 4; ###$P < 0.001$ versus control; and **$P < 0.001$ ML213 versus nifedipine + ML213, respectively; two-tailed paired Student's t-test). See Supplemental Fig. 3 for the display of summary responses as scatterplots with means.

the control (taken to be 100%) and expressed as percentages, with 100% indicating no effect and 0% indicating complete DSM relaxation.

Ratiometric Fluorescence Ca^{2+} Imaging. Global intracellular Ca^{2+} concentrations of isolated DSM strips were measured using the ratiometric fluorescence Ca^{2+} probe Fura-2 AM, as previously described (Hristov et al., 2012a; Provence et al., 2015).

Perforated Patch-Clamp Electrophysiology. K_V7 currents were recorded using the amphotericin-B perforated patch-clamp technique in voltage-clamp mode. At a holding potential of −10 mV (corrected for junction potential), K_V7 currents were recorded by applying 500-millisecond voltage steps at 10-mV intervals from voltages ranging from −80 to +40 mV. To effectively isolate K_V7 currents, recordings were made in the presence of the selective large-conductance voltage-activated and Ca^{2+}-activated K^+ (BK) channel inhibitor paxilline (1 μM) and $GdCl_3$ (50 μM), an inhibitor of nonselective cation channels and L-type voltage-gated Ca^{2+} channels (Mani et al., 2011; Brueggemann et al., 2012a). The amphotericin-B perforated patch-clamp technique in current-clamp mode ($I = 0$) was used to record the DSM cell membrane potential, as previously described (Afeli et al., 2013; Provence et al., 2015).

In Situ PLA. In situ PLA was performed on freshly isolated DSM cells using the Duolink In Situ Orange Starter Kit Goat/Rabbit (catalog #DUO92106; Sigma-Aldrich, St. Louis, MO) according to the manufacturer's instructions. DSM cells underwent fixation in 2% paraformaldehyde (10 minutes, 37°C) followed by two 15-minute washes in phosphate-buffered saline. DSM cells were then blocked in Duolink Blocking Solution (Sigma-Aldrich) (30 minutes, 37°C). Subsequently, DSM cells were incubated with the anti-rabbit $K_V7.4$ (catalog #sc-50417; Santa Cruz Biotechnology, Dallas, TX) and anti-goat $K_V7.5$ (catalog #sc-18048; Santa Cruz Biotechnology) antibodies or with the control anti-goat inositol triphosphate receptor (IP_3R) antibody (catalog #sc-28614; Santa Cruz Biotechnology), respectively, in Duolink antibody diluent solution overnight at 4°C, followed by 2× 5-minute washes in Duolink 1× Wash Buffer A Solution (Sigma-Aldrich). DSM cells were then incubated with the Duolink PLA Probe Anti-Rabbit MINUS and Anti-Goat PLUS oligonucleotide-conjugated secondary antibodies (Sigma-Aldrich) (1 hour, 37°C), followed by

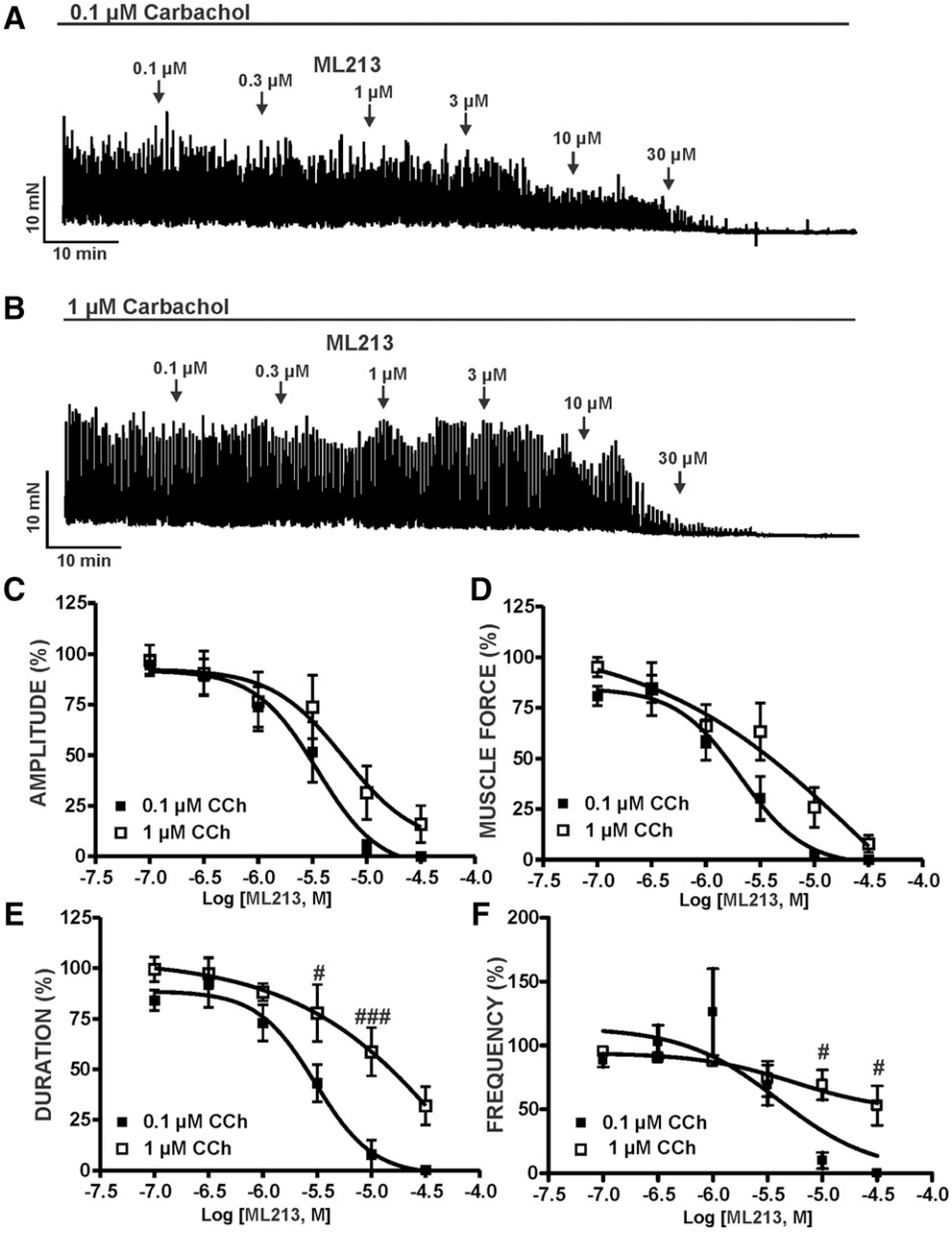

Fig. 4. K_V7 channel pharmacological activation with ML213 leads to an inhibition of CCh-induced DSM phasic contractions. (A) A representative isometric DSM tension recording demonstrating the concentration-dependent inhibition of 0.1 μM CCh-induced phasic contractions in a DSM isolated strip. (B) A representative isometric DSM tension recording demonstrating the concentration-dependent inhibition of 1 μM CCh-induced phasic contractions in a DSM isolated strip. Cumulative concentration-response curves for ML213 on CCh-induced (0.1 or 1 μM) DSM phasic contraction amplitude (C), muscle force (D), duration (E), and frequency (F) ($n = 6$, $N = 6$ for both data sets; #$P < 0.05$; ###$P < 0.001$; two-tailed paired Student's t-test). See Table 1 for potency and maximum efficacy values and Supplemental Fig. 4 for the illustration of summary concentration-responses, data for which are shown as the mean ± S.D. ANOVA analyses revealed significant differences for ML213-induced relaxation in the presence of 0.1 (micro)M CCh versus 1 (micro) M CCh for muscle force ($P = 0.006$) and duration ($P < 0.001$); for amplitude the difference just failed to reach significance ($P = 0.055$).

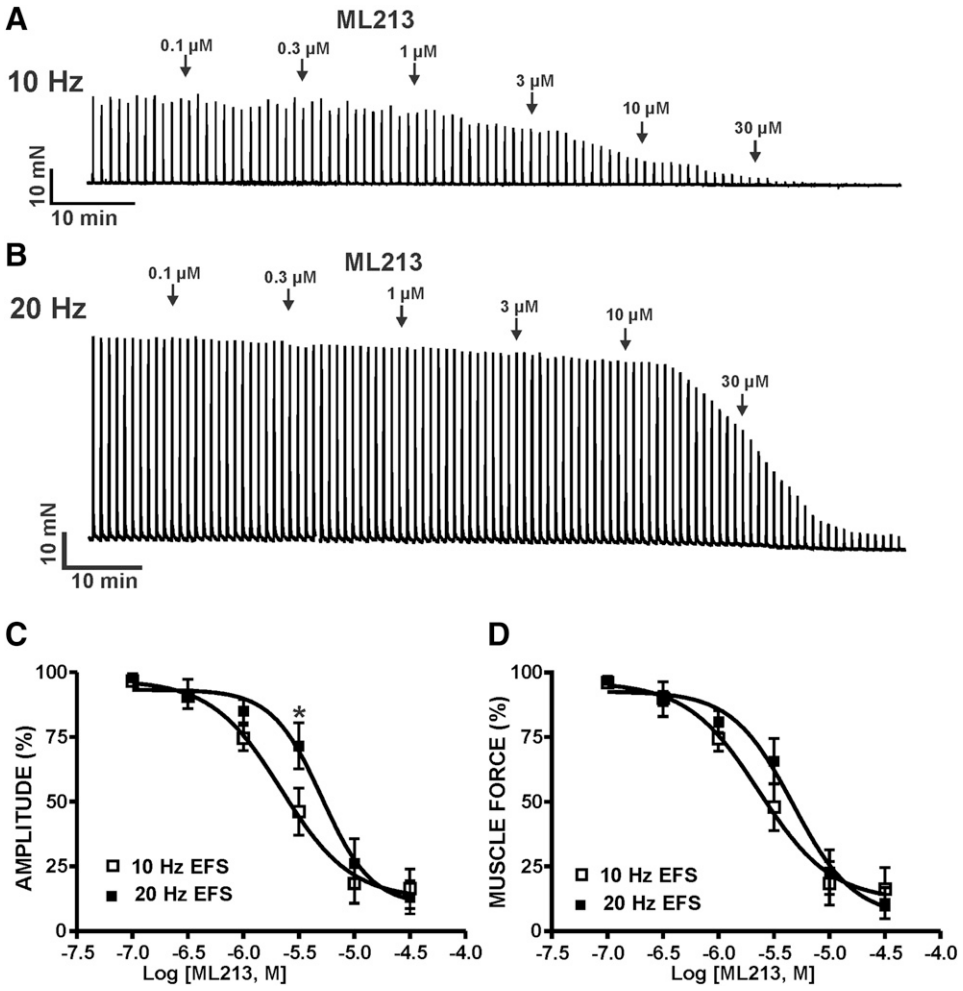

Fig. 5. K_V7 channel pharmacological activation with ML213 leads to an inhibition of nerve-evoked contractions induced by 10- and 20-Hz EFS in DSM isolated strips. (A) A representative isometric DSM tension recording demonstrating the concentration-dependent inhibition of 10 Hz EFS-induced contractions by ML213 (0.1–30 μM) in DSM isolated strips. (B) A representative isometric DSM tension recording illustrating the concentration-dependent inhibition of 20-Hz EFS-induced contractions by ML213 (0.1–30 μM) in DSM isolated strips. Cumulative concentration-response curves for ML213 on DSM EFS-induced contraction amplitude (C) and muscle force (D) (n = 7, N = 6 for 10 Hz; n = 6, N = 6 for 20 Hz; $^*P < 0.05$ for 10 versus 20 Hz; two-tailed paired Student's t-tests). See Table 1 for potency and maximum efficacy values and Supplemental Fig. 5 for illustration of summary concentration-responses, data for which are shown as the mean ± S.D.

2× 5-minute washes in Duolink 1× Wash Buffer A Solution (Sigma-Aldrich). DSM cells were then incubated in ligase-ligation solution (30 minutes, 37°C), which hybridizes the two PLA MINUS and PLUS probes when in close proximity (<40 nm). After ligation, DSM cells were washed 2× for 2 minutes in Duolink 1× Wash Buffer A solution. Finally, DSM cells were incubated in amplification-polymerase solution (100 minutes, 37°C) containing nucleotides and fluorescently labeled oligonucleotides. The oligonucleotide arm of one PLA probe is a primer for rolling-circle amplification. The fluorescently labeled oligonucleotides hybridize to the rolling circle amplification product thus permitting detection. After amplification, DSM cells were washed 2× 10 minutes in 1× wash buffer B and then a 1-minute wash in 0.01× wash buffer B. Slides were then mounted using minimal volume of Duolink In Situ Mounting Medium with 4′,6-diamidino-2-phenylindole dihydrochloride (Sigma-Aldrich). PLA signals (Duolink In Situ Detection Reagents Orange; Sigma-Aldrich) ($\lambda_{excitation/emission}$ = 554/576 nm) were detected using a laser-scanning LSM 700 Confocal Microscope (Carl Zeiss, Oberkochen, Germany) with a 63× oil-immersion objective.

Solutions and Drugs. Nominally Ca^{2+}-free dissection solution contained the following (in mM): 80 monosodium glutamate; 55 NaCl; 6 KCl; 10 glucose; 10 4-(2-hydroxyethyl) piperazine-1-ethanesulfonic acid (HEPES); 2 $MgCl_2$; NaOH was used to attain pH 7.3. Ca^{2+}-containing physiologic saline solution contained the following (millimolar): 119 NaCl; 4.7 KCl; 24 $NaHCO_3$; 1.2 KH_2PO_4; 2.5 $CaCl_2$; 1.2 $MgSO_4$; 11 glucose; aerated with 95% O_2/5% CO_2 to attain pH 7.4. Physiologic bath solution used for patch-clamp experiments was composed of the following (millimolar): 134 NaCl; 6 KCl; 1 $MgCl_2$; 2 $CaCl_2$; 10 glucose; and 10 HEPES; and NaOH was used to obtain pH 7.4. The patch-pipette solution contained the following (millimolar): 110 potassium aspartate; 30 KCl; 10 NaCl; 1 $MgCl_2$; and 10 HEPES; 0.05 EGTA; NaOH was used to adjust the pH to 7.2. Amphotericin-B stock solution was prepared daily in dimethylsulfoxide and was included in the pipette solution (200–300 μg/ml) before the experiment and was replaced every 1–2 hours. ML213, TTX citrate, and XE991 were purchased from Tocris Bioscience (Minneapolis, MN). Fura-2 AM was purchased from Life Technologies (catalog #F1221; Carlsbad, CA). ML213 and Fura-2 AM were dissolved in dimethylsulfoxide as stock solutions, whereas XE991 and TTX citrate were dissolved in double-distilled water. All other chemicals were obtained from Fisher Scientific (Waltham, MA), Sigma-Aldrich, or Worthington Biochemical Corp. (Lakewood, NJ).

Data Analysis and Statistics. Isometric DSM tension-recording experiments for spontaneous phasic, pharmacologically induced, and nerve-evoked contractions were conducted and analyzed as previously described (Hristov et al., 2012b; Afeli et al., 2013; Provence et al., 2015). Perforated whole-cell patch-clamp experiments were performed and analyzed using pCLAMP 10.3. Where specified in the summarized data, "n" represents the number of freshly isolated DSM strips or cells, and "N" represents the number of guinea pigs. Statistical analyses were based on n, the number of DSM cells or strips, respectively. For spontaneous contraction experiments, statistical analysis for the comparison of ML213 in the absence or presence of XE991, a two-way ANOVA test was performed followed by Bonferroni post hoc test. Paired Student's t-tests or Wilcoxon matched-pairs signed rank tests were used for the remaining statistical analyses. Summarized data are reported as the mean ± S.E.M. or medians with 25th and 75th percentiles. P values <0.05 (two tailed)

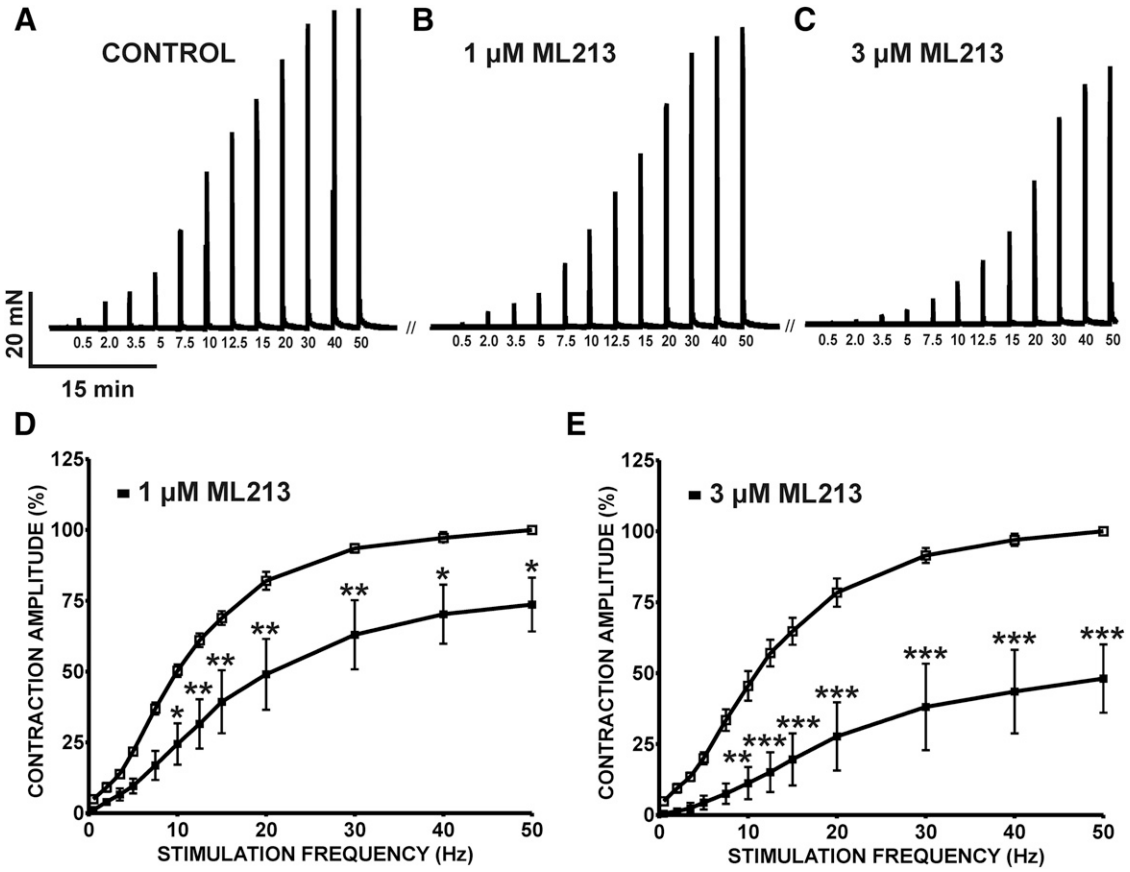

Fig. 6. ML213 decreases 0.5- to 50-Hz EFS-induced contractions in DSM isolated strips. The original isometric DSM tension recordings of 0.5- to 50-Hz EFS-induced contractions in DSM isolated strips before (control) (A) and after (B) the addition of 1 μM ML213 and 3 μM ML213 (C). Cumulative frequency-response curves demonstrating the inhibitory effects of 1 μM ML213 (D) and 3 μM ML213 (E) on the amplitude of 0.5- to 50-Hz EFS-induced contractions in DSM isolated strips (n = 6, N = 6 for both data sets; *$P < 0.05$; **$P < 0.01$; ***$P < 0.001$; two-tailed paired Student's t-test). See Supplemental Fig. 6 for the display of summary frequency-responses, data for which are shown as the mean ± S.D.

were considered to be statistically significant. CorelDRAW X3 Graphic Suite software (Corel Co., Mountain View, CA) and GraphPad Prism 4.03 or 7 software (GraphPad Software, La Jolla, CA) were used for data illustration and data analyses.

Results

ML213 Decreased Spontaneous Phasic Contractions in DSM Isolated Strips. To explore the physiologic effects of K_V7 channel pharmacological activation with ML213 on spontaneous phasic contractions, we conducted isometric DSM tension recordings on DSM isolated strips. ML213 (0.1–30 μM) caused a concentration-dependent inhibition of spontaneous phasic contractions in DSM isolated strips ($n = 6$, $N = 6$; $P < 0.05$) (Fig. 1; Supplemental Fig. 1). Pretreatment of DSM isolated strips with the K_V7 channel inhibitor XE991 (10 μM) abolished ML213-induced (0.1–30 μM) inhibition of spontaneous phasic contractions, confirming selectivity for K_V7 channels ($n = 6$, $N = 6$; $P < 0.05$) (Fig. 1; Supplemental Fig. 1). IC_{50} and maximal efficacy values for ML213 on spontaneous phasic contractions are reported in Table 1.

ML213 Decreased KCl-Induced Contractions in DSM Isolated Strips. Next, we elucidated the effects of ML213 (0.1–30 μM) on DSM contractions induced by mild membrane depolarization using 20 mM KCl. In the presence of 20 mM KCl, ML213 (0.1–30 μM) caused a concentration-dependent inhibition of DSM contractions and exhibited a decrease in potency in comparison with ML213 inhibitory effects on spontaneous phasic contractions (Table 1) ($n = 7$, $N = 7$; $P < 0.05$) (Fig. 2; Supplemental Fig. 2). To further explore the role of K^+ conductance in ML213-induced inhibition of DSM contractions and the potential direct interaction with L-type voltage-gated Ca^{2+} channels, we tested the effects of ML213 (10 μM) on tonic DSM contractions stimulated by high 60 mM KCl. Here, ML213 (10 μM) decreased 60 mM KCl-induced muscle tone to only 74% ± 3.5% of the control ($n = 8$, $N = 4$; $P < 0.01$) (Fig. 3; Supplemental Fig. 3). Subsequent application of the L-type voltage-gated Ca^{2+} channel inhibitor nifedipine, however, caused an inhibitory effect significantly greater in comparison with ML213 alone, decreasing DSM tone to 39.7% ± 6.4% of the control ($n = 8$, $N = 4$; $P < 0.001$) (Fig. 3; Supplemental Fig. 3). The difference between the inhibitory effects of ML213 (10 μM) and nifedipine in the presence of ML213 on tonic DSM contraction were statistically significant ($n = 8$, $N = 4$; $P < 0.001$) (Fig. 3; Supplemental Fig. 3). These data suggest that ML213 does not directly inhibit L-type voltage-gated Ca^{2+} channel activity in DSM.

CCh Attenuated ML213-Induced Inhibition of DSM Contractions in a Concentration-Dependent Manner. We next sought to determine the potential involvement of mAChR signaling in ML213-induced inhibition of DSM contractility. This was achieved by examining the inhibitory

effects of ML213 (0.1–30 μM) on DSM contractions stimulated by the mAChR agonist CCh (0.1 or 1 μM). ML213 (0.1–30 μM) caused a concentration-dependent inhibition of both 0.1 and 1 μM CCh ($n = 6$, $N = 6$ for both; $P < 0.05$) (Fig. 4; Supplemental Fig. 4). However, in comparison with 0.1 μM, mAChR stimulation with 1 μM CCh markedly reduced the potency of ML213 on DSM contraction duration and muscle force (Table 1). IC_{50} and maximal efficacy values for ML213 on 0.1 and 1 μM CCh-induced DSM contractions are reported in Table 1 (see also Fig. 4).

ML213 Decreased Nerve-Evoked Contractions in DSM Isolated Strips. To further explore potential roles for mAChRs in ML213-induced inhibition of DSM contractions, ML213 (0.1–30 μM) inhibitory effects were examined on nerve-evoked contractions stimulated by either 10- or 20-Hz EFS. ML213 (0.1–30 μM) caused a concentration-dependent inhibition of EFS-induced contractions stimulated continuously at both 10- and 20-Hz EFS frequencies ($n = 7, N = 6$ for 10 Hz; $n = 6, N = 6$ for 20 Hz) (Fig. 5; Supplemental Fig. 5). IC_{50} and maximal efficacy values for ML213 on 10- and 20-Hz EFS-induced contractions are reported in Table 1. In comparison with 10-Hz EFS, the potency of ML213 on 20-Hz EFS-induced contractions was reduced by more than 2-fold (see Table 1). Next, ML213 (1 or 3 μM) inhibitory effects were examined on contractions induced over a range of EFS frequencies (0.5–50 Hz). ML213 (1 or 3 μM) decreased the amplitude of 10- to 50-Hz EFS-induced contractions ($n = 6$, $N = 6$; $P < 0.05$) (Fig. 6; Supplemental Fig. 6).

ML213 Decreased Global Intracellular Ca^{2+} Concentrations in DSM Isolated Strips. We next aimed to assess the effects of ML213 on global intracellular Ca^{2+} concentrations of isolated DSM strips loaded with Fura-2. This was achieved using the ratiometric fluorescence Ca^{2+} indicator Fura-2 AM and measuring the emission at 510 nm with excitation at 340 and 380 nm. Under control conditions in the absence of ML213, the median intensity (F_{340}/F_{380}) was 0.85 (0.75–1.02, 25th to 75th percentiles) ($n = 8, N = 6$), and in the presence of ML213 (10 μM) the median F_{340}/F_{380} ratio decreased to a median of 0.78 (0.69–0.96) ($n = 8, N = 6; P < 0.01$) (Fig. 7; Supplemental Fig. 7). These results suggest that K_V7 channel pharmacological activation with ML213 critically regulates global intracellular Ca^{2+} concentrations in DSM isolated strips and thus DSM contractility.

ML213 Enhanced the Amplitude of Whole-Cell K_V7 Currents in Freshly Isolated DSM Cells. We next sought to examine the pharmacological effects of ML213 on whole-cell K_V7 currents using the perforated patch-clamp technique in voltage-clamp mode. In the first series of experiments, K_V7 currents were recorded at a holding potential of −10 mV wherein 500-millisecond voltage steps were applied at 10 mV intervals from −80 to +40 mV. To effectively isolate K_V7 currents, recordings were made in the presence of the selective BK channel inhibitor paxilline (1 μM) and $GdCl_3$ (50 μM), an inhibitor of nonselective cation and L-type voltage-gated Ca^{2+} channels. Further, the more depolarized holding potential of −10 mV that we used ensures inactivation of other non-K_V7 K^+ channels, such as inward-rectifying K^+ channels (Brueggemann et al., 2012b). ML213 (10 μM) caused a significant increase in the amplitude of whole-cell K_V7 currents at all voltages from −50 to +40 mV ($n = 7, N = 5$; $P < 0.05$) (Fig. 8). We further sought to examine the time course for the pharmacological effects of ML213 on K_V7 currents in DSM cells. This was achieved using a one-step voltage-clamp protocol with a 5-second duration stimulus applied every 20 seconds from a −10 mV holding potential to +40 mV. ML213 (10 μM) caused a significant increase in the whole-cell K_V7 current amplitude median values to 145.7% (125.3%–451.5%, 25th and 75th percentiles) and 132.1% (107.0%–159.2%, 25th and 75th percentiles), respectively, in comparison with the control ($n = 8, N = 5; P < 0.01$) (Fig. 9; Supplemental Fig. 9).

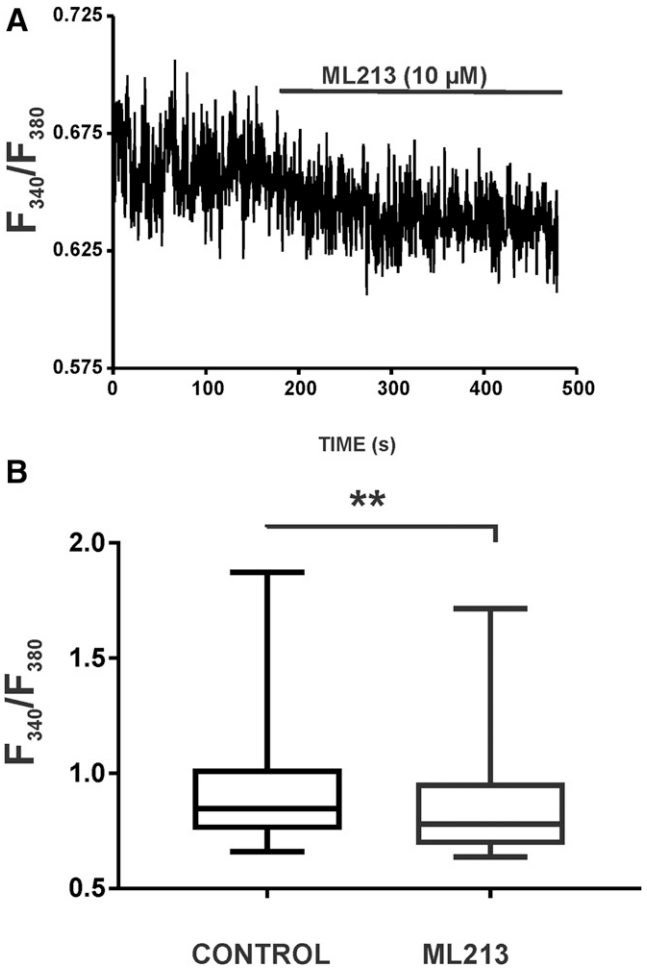

Fig. 7. ML213 decreases global intracellular Ca^{2+} concentrations in DSM isolated strips. (A) Original recordings illustrating that ML213 (10 μM) significantly decreased global intracellular Ca^{2+} levels in a Fura-2–loaded DSM strip. (B) Summarized data (as box-whisker plots) representing the reduction in global Ca^{2+} levels by 10 μM ML213 in DSM isolated strips ($n = 8, N = 6$; $^{**}P < 0.01$; two-tailed Wilcoxon matched-pairs signed rank test). See Supplemental Fig. 7 for the display of summary data as scatterplots with medians.

ML213 Hyperpolarizes the Resting Membrane Potential in Freshly Isolated DSM Cells. Using the perforated whole-cell patch-clamp technique in current-clamp mode, we next sought to determine the physiologic role of ML213-sensitive K_V7 channels in regulating the DSM cell membrane potential. ML213-induced inhibitory effects were examined in five DSM isolated cells from five different animals, which had an average resting membrane potential of −30.4 ± 6.2 mV. Subsequently, ML213 hyperpolarized the DSM cell membrane potential to −43.8 ± 5.0 mV ($n = 5, N = 5$; $P < 0.01$) (Fig. 10; Supplemental Fig. 10). ML213-induced DSM cell membrane hyperpolarization was fully reversible by

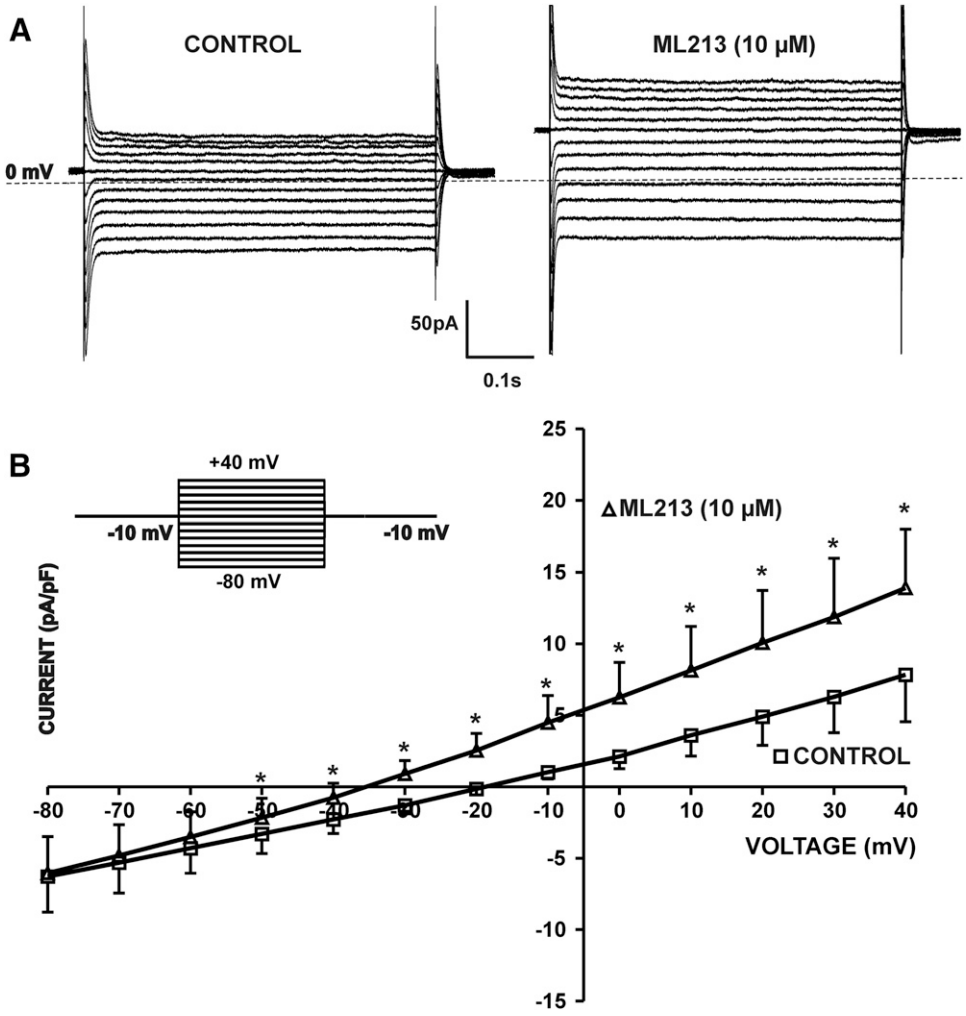

Fig. 8. ML213 (10 μM) enhanced whole-cell K_V7 currents in freshly isolated DSM cells. (A) Representative whole-cell patch-clamp recordings illustrating the potentiation of K_V7 currents induced by the introduction of ML213 in the bath external solution. Paxilline (1 μM) and $GdCl_3$ (50 μM) were present in the solution. (B) Current-voltage relationships obtained in the absence (control) or presence of 10 μM ML213 in a whole-cell voltage-clamp recording. The two curves represent the current-voltage relationship expressed as normalized current in the absence or presence of 10 μM ML213 (n = 7, N = 5, $^*P <$ 0.05; two-tailed paired Student's t-test). (B, top left insert) The 500-millisecond voltage-step protocol from −80 to +40 mV with a holding potential at −10 mV. See Supplemental Fig. 8 for current-voltage plots, data for which are shown as the mean ± S.D.

washout of ML213 (Fig. 10, A and B; Supplemental Fig. 10A). On the contrary, XE991 (10 μM) depolarized the DSM cell membrane potential from −29.8 ± 4.3 to −18.7 ± 2.7 mV and blocked ML213 (10 μM) hyperpolarization at −20.6 ± 2.8 mV ($n = 8, N = 4; P < 0.05$) (Fig. 10, C and D; Supplemental Fig. 10B), confirming ML213 selectivity for the K_V7 channels. XE991 (10 μM) was also effective in reversing the hyperpolarizing effects of ML213 from −39.2 ± 9.2 to −23.2 ± 5.5 mV (control was −26.6 ± 7.2 mV) (n = 7, N = 6; $P < 0.05$) (Fig. 11; Supplemental Fig. 11). These combined results suggest key involvement for ML213-sensitive $K_V7.2$, $K_V7.4$, and $K_V7.5$ channels in regulating the DSM cell membrane potential.

$K_V7.4$ and $K_V7.5$ Channel α-Subunits Assemble to Form Heteromeric $K_V7.4/K_V7.5$ Channel Subtypes in Freshly Isolated DSM Cells. Using in situ PLA, we sought to determine whether $K_V7.4$ and $K_V7.5$ channels, among the key targets of ML213, form heteromeric channels in freshly isolated DSM cells. In situ PLA demonstrated that $K_V7.4$ and $K_V7.5$ channel subunits associate to form heteromeric $K_V7.4/K_V7.5$ channels in isolated DSM cells. As shown in Fig. 12, in situ PLA experiments demonstrated the colocalization of $K_V7.4$ and $K_V7.5$ channel α-subunits within 40 nm and within the vicinity of the DSM cell membrane. Primary antibodies against the IP_3R, which would not be expected to colocalize with members of the K_V7 channel family, were used as a negative control. Coincubation of the $K_V7.4$ channel primary antibody with the primary antibody of the IP_3Rs yielded no PLA fluorescent signal (Fig. 12). These combined results suggest that $K_V7.4$ and $K_V7.5$ channel subunits assemble to form heteromeric $K_V7.4/K_V7.5$ channel subtypes in DSM cells.

Discussion

The current study used the novel compound ML213, a potent and selective activator of $K_V7.2$-, $K_V7.4$-, and $K_V7.5$-containing channels, to elucidate their physiologic roles in DSM function. ML213 inhibited spontaneous, pharmacologically induced, and nerve-evoked DSM contractions and decreased global intracellular Ca^{2+} concentrations in DSM strips. ML213 enhanced whole-cell K_V7 currents and hyperpolarized the resting membrane potential of freshly isolated DSM cells. In situ PLA studies further revealed the expression of heteromeric $K_V7.4/K_V7.5$ channels within the vicinity of the DSM cell membrane.

Previous studies on guinea pig, including those from our group, demonstrated a role for K_V7 channels in DSM function (Afeli et al., 2013; Anderson et al., 2013; Provence et al., 2015). Here, ML213 promoted concentration-dependent inhibition of spontaneous phasic contractions with IC_{50} values of 1.1 and

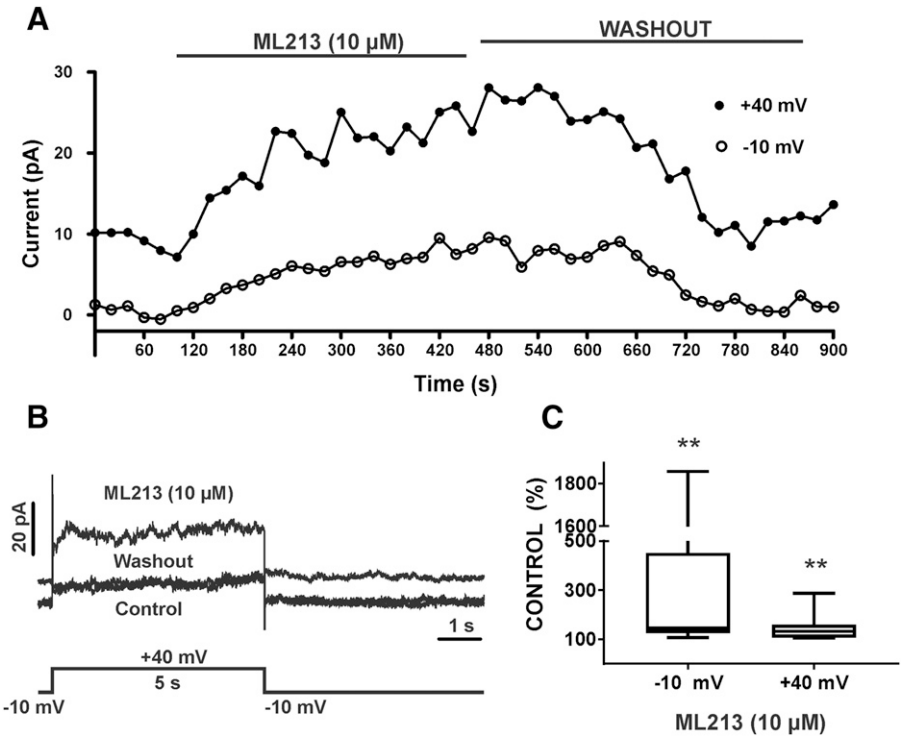

Fig. 9. Time course of ML213-induced activation of K_V7 channel currents in freshly isolated DSM cells. (A) Effects of ML213 on K_V7 currents recorded using a one-step voltage-clamp protocol with a 5-second duration stimulus applied every 20 seconds from a −10-mV holding potential to +40 mV. (B) Representative traces (and voltage step used) of the experiment plotted in (A) for the control, ML213 (10 μM), and washout of ML213. (C) Summary data for the percentage of K_V7 currents in the presence of ML213 compared with control at −10 and +40 mV, respectively (n = 8, N = 5, $^{**}P < 0.01$; two-tailed Wilcoxon matched-pairs signed rank test). Summarized data illustrate the average of four to six points of each steady-state current. See Supplemental Fig. 9 for display of summary data as scatterplots with medians.

0.7 μM, respectively (Fig. 1; Table 1). The observed inhibitory effects of ML213 on DSM contractile activity are consistent with previous reports in human and pig DSM (Svalø et al., 2013, 2015; Bientinesi et al., 2017). Based on our data, ML213 displays greater potency in comparison with retigabine, the $K_V7.1$ channel activator L-364373, and the $K_V7.2/K_V7.3$ channel activator ICA-069673 for inhibiting DSM spontaneous phasic contraction amplitude and muscle force (Afeli et al., 2013; Anderson et al., 2013; Provence et al., 2015).

ICA-069673 and ML213 are known to potently activate homomeric $K_V7.4$ channels; however, the key distinction between these two compounds is the ability for ML213 to potently activate both homomeric $K_V7.5$ and heteromeric $K_V7.4/K_V7.5$ channels (Brueggemann et al., 2014a). The greater potency for ML213 to inhibit spontaneous phasic, pharmacologically induced, and EFS-induced DSM contractions (Figs. 1–6), in comparison with ICA-069673 (Provence et al., 2015), supports the involvement of $K_V7.4$- or $K_V7.5$-containing channels in DSM function. Similar observations were reported using ML213 in rodent mesenteric arteries, where the $K_V7.4$ channels subtypes are predominately expressed (Jepps et al., 2014).

ML213 inhibited DSM contractions induced by the mAChR agonist CCh in a concentration-dependent manner (Fig. 4). Consistently, ML213 exhibited a reduced effect on amplitude for 20-Hz EFS-induced DSM contractions in comparison with 10-Hz contractions (Fig. 5). ML213 inhibitory effects on CCh- and EFS-induced DSM contractions are in line with previous reports in pigs and humans (Svalø et al., 2013, 2015). These results suggest that cellular pathways leading to the activation K_V7 channels may function in opposition to mAChR signaling. However, confirming the existence of a functional link between K_V7 channels and mAChRs in DSM requires future studies. Parasympathetic nerves release ACh and ATP, which act on mAChRs and purinergic receptors, respectively, to trigger urinary bladder smooth muscle contraction during micturition (Andersson and Arner, 2004; Werner et al., 2007; Heppner et al., 2009), with ACh-induced activation of mAChRs being the primary mechanism (Andersson and Arner, 2004). EFS evokes ACh release from parasympathetic nerve terminals, which leads to depolarization of the DSM cell membrane potential and associated DSM contractions (Nausch et al., 2010). Although mAChR regulation of K_V7 channel activity is consistent with early studies in neurons (Brown et al., 1980), whether a similar regulatory mechanism exists in DSM remains unknown. A recent study in airway smooth muscle reported that, unlike neuronal K_V7 channels (Delmas and Brown, 2005), mAChR activation by CCh did not exhibit significant inhibitory effects on K_V7 currents (Evseev et al., 2013). Thus, K_V7 channel activation in DSM may act in opposition to mAChRs through an indirect mechanism, for example, the modulation of L-type voltage-gated Ca^{2+} channels. Consistent with ML213 inhibitory effects on DSM contractions, we further observed attenuation of global intracellular Ca^{2+} concentrations by ML213 in DSM strips (Fig. 7).

For the first time, we report the activation of whole-cell K_V7 currents by ML213 in freshly isolated DSM cells (Figs. 8 and 9). The use of a more depolarized holding potential (−10 mV) in our study ensured inactivation of other non-K_V7 K^+ channels, such as inward-rectifying K^+ channels (Brueggemann et al., 2012b). Also, at a −10-mV holding potential, some of the K_V7 channels are open and generate quantifiable currents, which are not contaminated by the presence of nonselective cation currents due to the inclusion of $GdCl_3$. Thus, the stimulatory effects of ML213 on K_V7 currents are evident (Fig. 8; Supplemental Fig. 8). Our data support the

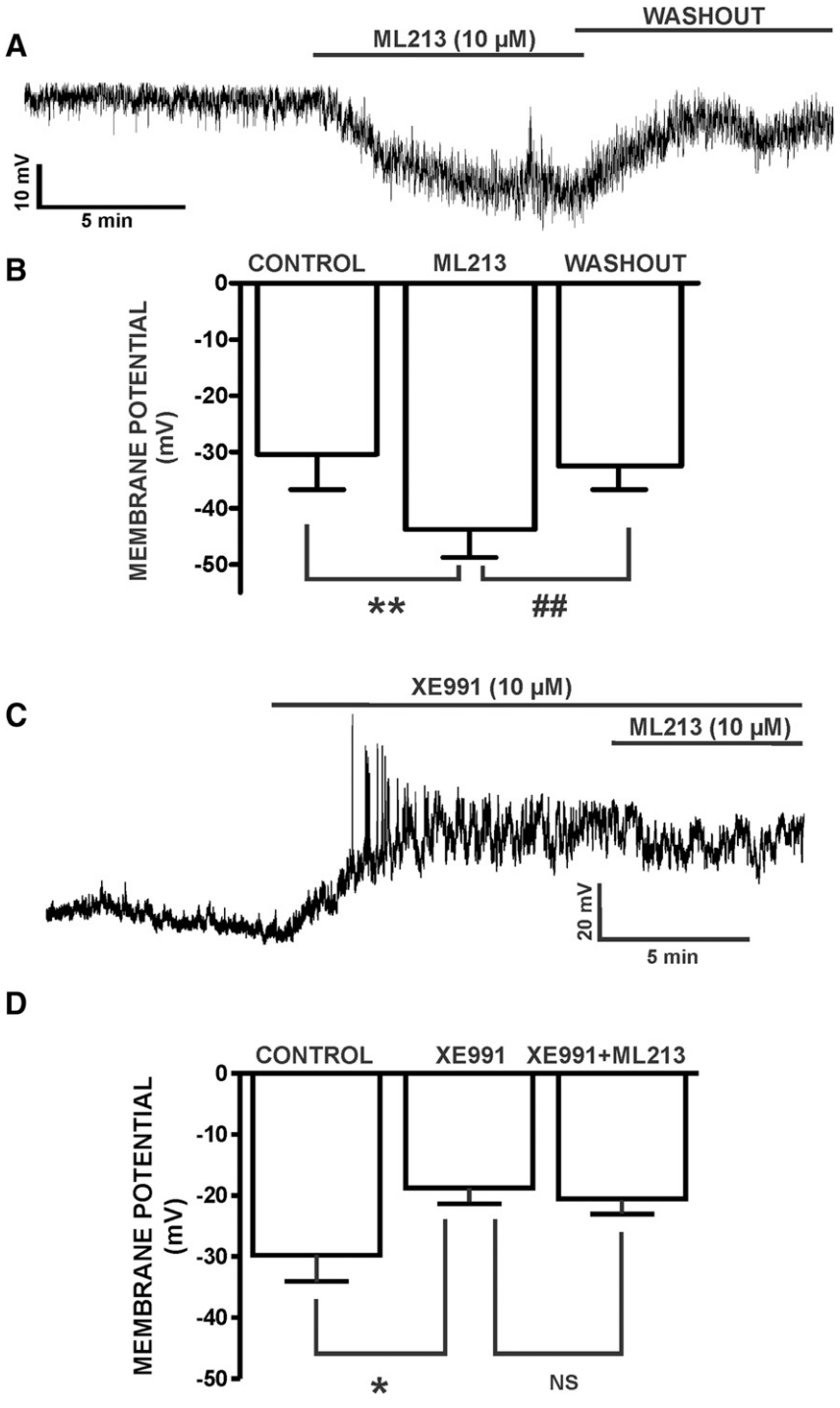

Fig. 10. ML213 hyperpolarizes the resting membrane potential in freshly isolated DSM cells. (A) A representative membrane potential recording in current-clamp mode illustrating that ML213 (10 μM) hyperpolarized the DSM cell membrane potential in a freshly isolated DSM cell and that this effect was reversible by washout. (B) Summarized data for the hyperpolarizing effects of ML213 (10 μM) on the DSM cell membrane potential ($n = 5, N = 5$; $^{**}P < 0.01$) and for the washout ($n = 5, N = 5, \#\#P < 0.01$). (C) A representative membrane potential recording in current-clamp mode demonstrating that XE991 (10 μM) depolarized the DSM cell membrane potential and blocked ML213 (10 μM) hyperpolarization in a freshly isolated DSM cell. (D) Summarized data for XE991-induced (10 μM) depolarization in freshly isolated DSM cells and the lack of ML213 (10 μM) hyperpolarizing effects in the presence of 10 μM XE991 ($n = 8$, $N = 4$; $^{*}P < 0.05$; two-tailed paired Student's t-test), NS, nonsignificant. See Supplemental Fig. 10 for display of summary data as scatterplots with means.

concept that the hyperpolarizing currents after the addition of ML213 are a direct result of K_V7 channel pharmacological activation. In a series of experiments, marginal kinetics of voltage dependence of activation of K_V7 channels were revealed using a short–voltage step (500-millisecond) protocol. Longer voltage step protocols (5 seconds) with multiple voltage steps may result in time-dependent rundown after several minutes of recording. Hence, we sought to examine the time course effects of ML213 on K_V7 current activity by performing a one-step 5-second voltage-clamp protocol from a holding potential of −10 mV to one of +40 mV at 20-second intervals (Fig. 9). This protocol allowed for the recording of K_V7 channel currents without encountering substantial current rundown. The stimulatory effects of ML213 on K_V7 currents were modest but statistically significant (Figs. 8 and 9), although it is well established that small changes in DSM cell excitability can have pronounced effects on DSM contractility (Petkov et al., 2001; Petkov, 2014). Indeed, we observed very robust ML213 inhibitory effects on DSM contractility (Figs. 1–4). Overall, the experimental design for our electrophysiological experiments aimed not only to examine K_V7 current activity and its response to pharmacological

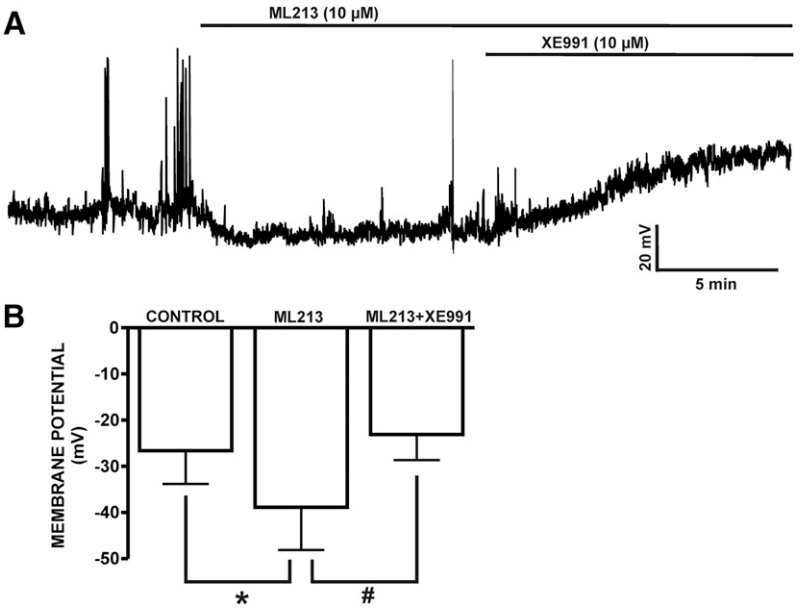

Fig. 11. ML213-induced hyperpolarization is reversed by K_V7 channel inhibition with XE991. (A) A representative current-clamp recording from a freshly isolated DSM cell illustrating hyperpolarization of the DSM cell membrane potential by ML213 (10 μM) and that the ML213-induced hyperpolarization is reversed by the K_V7 channel inhibitor XE991 (10 μM). (B) Summary data for the hyperpolarizing effects of ML213 (10 μM) on the DSM cell membrane potential ($n = 7, N = 5, {}^*P < 0.05$) effects reversible by 10 μM XE991 ($n = 7, N = 5; \#P < 0.05$; two-tailed paired Student's t-test). See Supplemental Fig. 11 for display of summary data as scatterplots with means.

activation with ML213, but also to mimic a physiologic environment characterized by a more depolarized resting membrane potential, which normally occurs during the action potential. Activation of ML213-sensitive K_V7 channels was further shown to hyperpolarize the DSM cell membrane potential (Fig. 10), consistent with ML213 inhibitory effects on global intracellular Ca^{2+} concentrations and DSM contractility.

K_V7 channel α-subunits are known to form functional homomeric and heteromeric channel conformations in vitro and in vivo (Soldovieri et al., 2011; Stott et al., 2014), with $K_V7.4$ and $K_V7.5$ being prominent in smooth muscle tissues (Gamper and Shapiro, 2015). In vascular myocytes, ML213 has been shown to activate heteromeric $K_V7.4/K_V7.5$ channels in addition to the homomeric channels composed of either $K_V7.4$ or $K_V7.5$ channel α-subunits (Yu et al., 2010;

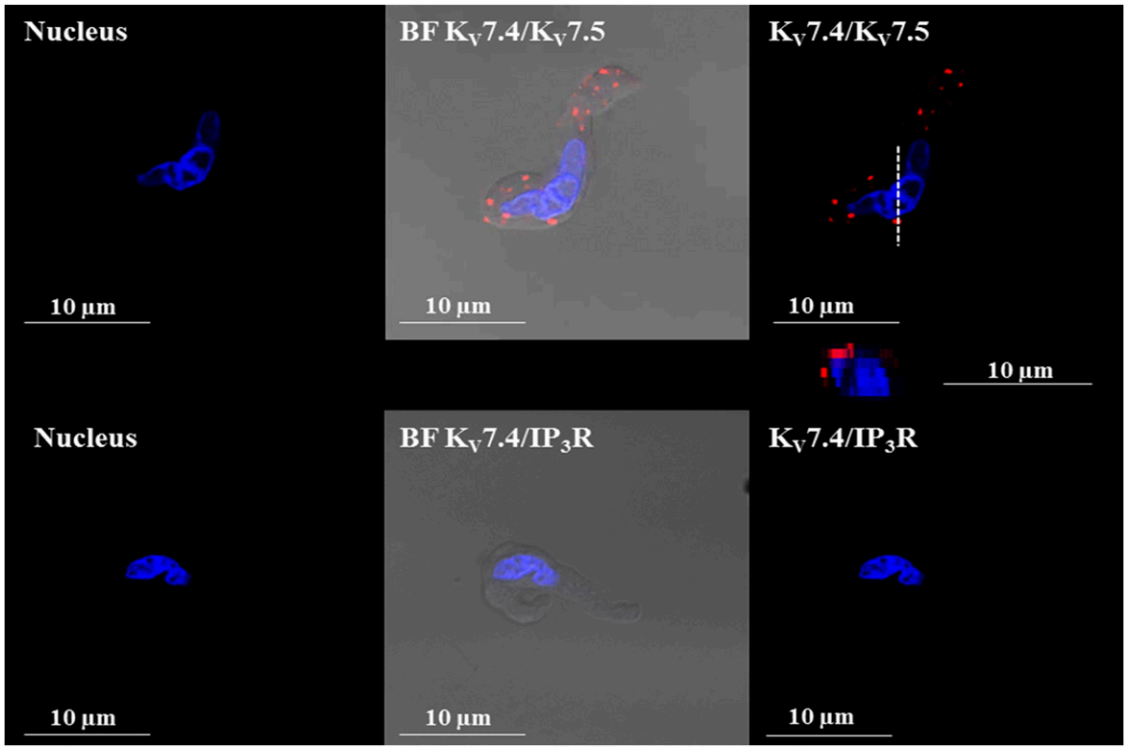

Fig. 12. PLA shows that $K_V7.4/K_V7.5$ heteromeric channels are expressed in isolated guinea pig DSM cells. Images of a freshly isolated DSM cell stained with the combination of anti-$K_V7.4$ and anti-$K_V7.5$ channel antibodies (top panels). PLA fluorescent signals are shown in red. No PLA fluorescent signals were observed when the anti-$K_V7.4$ antibody was coincubated with the anti-IP_3R antibody (bottom panels). An orthogonal cross-sectional image of the DSM cell displaying PLA signals was obtained after z-stack scans collected along the viewing plane indicated by the dashed (- - -) lines and is represented directly below the top right panel. BF, bright field; DAPI, 4′,6-diamidine-2′-phenylindole dihydrochloride (nuclear staining shown in blue).

Brueggemann et al., 2014a). In addition to $K_V7.2$ channel expression in guinea pig DSM (Afeli et al., 2013; Anderson et al., 2013; Provence et al., 2015), $K_V7.4$ (Anderson et al., 2013) and $K_V7.5$ (Afeli et al., 2013; Anderson et al., 2013) channel α-subunits have been identified. However, whether these K_V7 channel subunits, in particular $K_V7.4$ or $K_V7.5$, associate to form functional heteromers in DSM remained unknown until now. We confirmed the expression of heteromeric $K_V7.4/K_V7.5$ channels in isolated DSM cells using in situ PLA. PLA fluorescent signals for $K_V7.4/K_V7.5$ α-subunit colocalization were uniformly detected through the DSM cell periphery, suggesting their plasmalemmal expression (Fig. 12). These findings, which are consistent with studies on rodent vasculature (Chadha et al., 2014), provide strong evidence confirming heteromeric $K_V7.4/K_V7.5$ channel expression in DSM cells. Although heteromeric $K_V7.4/K_V7.5$ channels are potently activated by ML213 pharmacological activation, it has not yet been reported whether heteromeric $K_V7.2/K_V7.3$ channels or other $K_V7.2$-containing channels, are ML213 sensitive. However, the potential activation of $K_V7.2/K_V7.3$ channels, for example, by ML213, would presumably be mediated by the $K_V7.2$ channel subunit because $K_V7.3$ channel subtypes are insensitive to ML213.

In addition, further studies to elucidate the precise stoichiometry of K_V7 channels and their associations with β-regulatory subunits (KCNE1–5, (beta) accessory subunits of Kv7 channels) will be required to further understand the potential ML213 targets in DSM. Indeed, a recent study (Jepps et al., 2015) in rodent arterial myocytes demonstrated KCNE4 colocalization with $K_V7.4$ and $K_V7.5$ channels, respectively. Also, the coexpression of KCNE4 with $K_V7.4$ channels was found to increase $K_V7.4$ channel expression and current amplitudes (Jepps et al., 2015). Moreover, a report from bovine DSM suggests that $K_V7.4$ channel subtypes are the most abundantly expressed; findings consistent with emerging studies in humans demonstrating $K_V7.4$ mRNA expression as the primary K_V7 channel expressed in DSM (Svalø et al., 2015; Bientinesi et al., 2017). A separate group reported $K_V7.5$ channel mRNA expression as the most highly expressed K_V7 channel subtype in human DSM (Argentieri et al., 2002). Although ML213 and ICA-069673 activate $K_V7.2$ channels, their differential selectivity for $K_V7.4$- and $K_V7.5$-containing channels demonstrates the capacity for subtype-specific pharmacological targeting.

Because our in situ PLA experiments provided decisive evidence confirming the expression of heteromeric $K_V7.4/K_V7.5$ channel subtypes in DSM (Fig. 12), these channels may be among the key pharmacological targets for ML213. However, homomeric $K_V7.4$ and $K_V7.5$ channel subtypes may also be critically involved as a previous report revealed ML213 to be equally potent for $K_V7.4$- and $K_V7.5$-containing channels (Brueggemann et al., 2014a). The ability to fine-tune K_V7 channel pharmacological modulators to exhibit improved selectivity among $K_V7.4$, $K_V7.5$, and $K_V7.4/K_V7.5$ channels may represent a substantial breakthrough in the development of novel and efficacious therapeutic modalities for lower urinary tract dysfunction.

In conclusion, our study demonstrates that ML213-sensitive $K_V7.4$- and $K_V7.5$-containing channels are essential regulators of DSM excitability and contractility. K_V7 channel activation by the novel activator ML213 leads to the activation of K_V7 currents, hyperpolarization of the membrane potential, a decrease in global intracellular Ca^{2+} concentration, and the attenuation of DSM contractility.

Acknowledgments

We thank Dr. James W. Hardin for the critical evaluation of our data and statistical methods. We also thank Dr. Kiril L. Hristov for help with some of the experiments; and Dr. Whitney Kellett, Dr. John Malysz, Dr. Viktor Yarotskyy, and Ms. Sarah Maxwell for critical evaluation of the manuscript.

Authorship Contributions

Participated in research design: Provence, Angoli, and Petkov.
Conducted experiments: Provence, Angoli, and Petkov.
Performed data analysis: Provence, Angoli, and Petkov.
Wrote or contributed to the writing of the manuscript: Provence, Angoli, and Petkov.

References

Abbott GW and Goldstein SA (2001) Potassium channel subunits encoded by the KCNE gene family: physiology and pathophysiology of the MinK-related peptides (MiRPs). *Mol Interv* **1**:95–107.
Afeli SA, Malysz J, and Petkov GV (2013) Molecular expression and pharmacological evidence for a functional role of k_v7 channel subtypes in Guinea pig urinary bladder smooth muscle. *PLoS One* **8**:e75875.
Anderson UA, Carson C, Johnston L, Joshi S, Gurney AM, and McCloskey KD (2013) Functional expression of KCNQ (K_v7) channels in guinea pig bladder smooth muscle and their contribution to spontaneous activity. *Br J Pharmacol* **169**: 1290–1304.
Andersson KE and Arner A (2004) Urinary bladder contraction and relaxation: physiology and pathophysiology. *Physiol Rev* **84**:935–986.
Argentieri T, Sheldon J, and Bowlby M (2002) inventors, American Home Products Corporation, assignee. Methods for modulating bladder function. U.S. patent 6,348,486. 2002 Feb 19.
Barhanin J, Lesage F, Guillemare E, Fink M, Lazdunski M, and Romey G (1996) K(V) LQT1 and lsK (minK) proteins associate to form the I(Ks) cardiac potassium current. *Nature* **384**:78–80.
Bientinesi R, Mancuso C, Martire M, Bassi PF, Sacco E, and Currò D (2017) K_V7 channels in the human detrusor: channel modulator effects and gene and protein expression. *Naunyn Schmiedebergs Arch Pharmacol* **390**:127–137.
Brown AM, Akaike N, Tsuda Y, and Morimoto K (1980) Ion migration and inactivation in the calcium channel. *J Physiol (Paris)* **76**:395–402.
Brown DA and Passmore GM (2009) Neural KCNQ (K_v7) channels. *Br J Pharmacol* **156**:1185–1195.
Brueggemann LI, Haick JM, Cribbs LL, and Byron KL (2014a) Differential activation of vascular smooth muscle Kv7.4, Kv7.5, and Kv7.4/7.5 channels by ML213 and ICA-069673. *Mol Pharmacol* **86**:330–341.
Brueggemann LI, Haick JM, Neuburg S, Tate S, Randhawa D, Cribbs LL, and Byron KL (2014b) KCNQ (Kv7) potassium channel activators as bronchodilators: combination with a β2-adrenergic agonist enhances relaxation of rat airways. *Am J Physiol Lung Cell Mol Physiol* **306**:L476–L486.
Brueggemann LI, Kakad PP, Love RB, Solway J, Dowell ML, Cribbs LL, and Byron KL (2012a) Kv7 potassium channels in airway smooth muscle cells: signal transduction intermediates and pharmacological targets for bronchodilator therapy. *Am J Physiol Lung Cell Mol Physiol* **302**:L120–L132.
Brueggemann LI, Mani BK, Haick J, and Byron KL (2012b) Exploring arterial smooth muscle K_v7 potassium channel function using patch clamp electrophysiology and pressure myography. *J Vis Exp* (67):e4263.
Chadha PS, Jepps TA, Carr G, Stott JB, Zhu HL, Cole WC, and Greenwood IA (2014) Contribution of $k_v7.4/k_v7.5$ heteromers to intrinsic and calcitonin gene-related peptide-induced cerebral reactivity. *Arterioscler Thromb Vasc Biol* **34**:887–893.
Delmas P and Brown DA (2005) Pathways modulating neural KCNQ/M (Kv7) potassium channels. *Nat Rev Neurosci* **6**:850–862.
Evseev AI, Semenov I, Archer CR, Medina JL, Dube PH, Shapiro MS, and Brenner R (2013) Functional effects of KCNQ $K^{(+)}$ channels in airway smooth muscle. *Front Physiol* **4**:277.
Gamper N and Shapiro MS (2015) KCNQ channels, in *Handbook of Ion Channels* (Zheng J and Trudeau M eds) pp 275–306, CRC Press, Boca Raton, FL.
Haick JM and Byron KL (2016) Novel treatment strategies for smooth muscle disorders: targeting K_v7 potassium channels. *Pharmacol Ther* **165**:14–25.
Heppner TJ, Werner ME, Nausch B, Vial C, Evans RJ, and Nelson MT (2009) Nerve-evoked purinergic signalling suppresses action potentials, Ca^{2+} flashes and contractility evoked by muscarinic receptor activation in mouse urinary bladder smooth muscle. *J Physiol* **587**:5275–5288.
Hristov KL, Chen M, Afeli SA, Cheng Q, Rovner ES, and Petkov GV (2012a) Expression and function of $K_{(V)}2$-containing channels in human urinary bladder smooth muscle. *Am J Physiol Cell Physiol* **302**:C1599–C1608.
Hristov KL, Chen M, Soder RP, Parajuli SP, Cheng Q, Kellett WF, and Petkov GV (2012b) $K_V2.1$ and electrically silent K_V channel subunits control excitability and contractility of guinea pig detrusor smooth muscle. *Am J Physiol Cell Physiol* **302**: C360–C372.

Jepps TA, Bentzen BH, Stott JB, Povstyan OV, Sivaloganathan K, Dalby-Brown W, and Greenwood IA (2014) Vasorelaxant effects of novel K_v 7.4 channel enhancers ML213 and NS15370. *Br J Pharmacol* **171**:4413–4424.

Jepps TA, Carr G, Lundegaard PR, Olesen SP, and Greenwood IA (2015) Fundamental role for the KCNE4 ancillary subunit in K_v7.4 regulation of arterial tone. *J Physiol* **593**:5325–5340.

Jepps TA, Greenwood IA, Moffatt JD, Sanders KM, and Ohya S (2009) Molecular and functional characterization of K_v7 K^+ channel in murine gastrointestinal smooth muscles. *Am J Physiol Gastrointest Liver Physiol* **297**:G107–G115.

Mani BK, Brueggemann LI, Cribbs LL, and Byron KL (2011) Activation of vascular KCNQ (Kv7) potassium channels reverses spasmogen-induced constrictor responses in rat basilar artery. *Br J Pharmacol* **164**:237–249.

Mani BK, O'Dowd J, Kumar L, Brueggemann LI, Ross M, and Byron KL (2013) Vascular KCNQ (K_v7) potassium channels as common signaling intermediates and therapeutic targets in cerebral vasospasm. *J Cardiovasc Pharmacol* **61**:51–62.

Mani BK, Robakowski C, Brueggemann LI, Cribbs LL, Tripathi A, Majetschak M, and Byron KL (2016) K_v7.5 potassium channel subunits are the primary targets for PKA-dependent enhancement of vascular smooth muscle K_v7 currents. *Mol Pharmacol* **89**:323–334.

Nausch B, Heppner TJ, and Nelson MT (2010) Nerve-released acetylcholine contracts urinary bladder smooth muscle by inducing action potentials independently of IP_3-mediated calcium release. *Am J Physiol Regul Integr Comp Physiol* **299**:R878–R888.

Ng FL, Davis AJ, Jepps TA, Harhun MI, Yeung SY, Wan A, Reddy M, Melville D, Nardi A, Khong TK, et al. (2011) Expression and function of the K+ channel KCNQ genes in human arteries. *Br J Pharmacol* **162**:42–53.

Petkov GV (2011) Role of potassium ion channels in detrusor smooth muscle function and dysfunction. *Nat Rev Urol* **9**:30–40.

Petkov GV (2014) Central role of the BK channel in urinary bladder smooth muscle physiology and pathophysiology. *Am J Physiol Regul Integr Comp Physiol* **307**:R571–R584.

Petkov GV, Heppner TJ, Bonev AD, Herrera GM, and Nelson MT (2001) Low levels of K(ATP) channel activation decrease excitability and contractility of urinary bladder. *Am J Physiol Regul Integr Comp Physiol* **280**:R1427–R1433.

Provence A, Malysz J, and Petkov GV (2015) The novel K_V7.2/K_V7.3 channel opener ICA-069673 reveals subtype-specific functional roles in guinea pig detrusor smooth muscle excitability and contractility. *J Pharmacol Exp Ther* **354**:290–301.

Rode F, Svalø J, Sheykhzade M, and Rønn LC (2010) Functional effects of the KCNQ modulators retigabine and XE991 in the rat urinary bladder. *Eur J Pharmacol* **638**:121–127.

Soldovieri MV, Miceli F, and Taglialatela M (2011) Driving with no brakes: molecular pathophysiology of K_v7 potassium channels. *Physiology (Bethesda)* **26**:365–376.

Stott JB, Jepps TA, and Greenwood IA (2014) K(V)7 potassium channels: a new therapeutic target in smooth muscle disorders. *Drug Discov Today* **19**:413–424.

Streng T, Christoph T, and Andersson KE (2004) Urodynamic effects of the K^+ channel (KCNQ) opener retigabine in freely moving, conscious rats. *J Urol* **172**: 2054–2058.

Svalø J, Bille M, Parameswaran Theepakaran N, Sheykhzade M, Nordling J, and Bouchelouche P (2013) Bladder contractility is modulated by K_v7 channels in pig detrusor. *Eur J Pharmacol* **715**:312–320.

Svalø J, Sheykhzade M, Nordling J, Matras C, and Bouchelouche P (2015) Functional and molecular evidence for K_v7 channel subtypes in human detrusor from patients with and without bladder outflow obstruction. *PLoS One* **10**:e0117350.

Werner ME, Knorn AM, Meredith AL, Aldrich RW, and Nelson MT (2007) Frequency encoding of cholinergic- and purinergic-mediated signaling to mouse urinary bladder smooth muscle: modulation by BK channels. *Am J Physiol Regul Integr Comp Physiol* **292**:R616–R624.

Wrobel E, Tapken D, and Seebohm G (2012) The KCNE tango–how KCNE1 interacts with Kv7.1. *Front Pharmacol* **3**:142.

Yu H, Wu M, Hopkins C, Engers J, Townsend S, Lindsley C, McManus OB, and Li M (2011) A small molecule activator of KCNQ2 and KCNQ4 channels, in *Probe Reports from the NIH Molecular Libraries Program*, National Center for Biotechnology Information 2010-, Bethesda, MD.

Yu H, Wu M, Townsend SD, Zou B, Long S, Daniels JS, McManus OB, Li M, Lindsley CW, and Hopkins CR (2011) Discovery, synthesis, and structure activity relationship of a series of N-aryl-bicyclo[2.2.1]heptane-2-carboxamides: characterization of ML213 as a novel KCNQ2 and KCNQ4 potassium channel opener. *ACS Chem Neurosci* **2**:572–577.

Address correspondence to: Dr. Georgi V. Petkov, Department of Pharmaceutical Sciences, College of Pharmacy, The University of Tennessee Health Science Center, Pharmacy Building, Room 551, 881 Madison Avenue, Memphis, TN 38163. E-mail: gpetkov@uthsc.edu